Spectrochimica Acta Part A: Molecular and Biomolecular Spectroscopy 135 (2015) 1011–1018

Contents lists available at ScienceDirect

Spectrochimica Acta Part A: Molecular and Biomolecular Spectroscopy

journal homepage: www.elsevier.com/locate/saa

Synthesis, characterization and theoretical studies of 5-(benzylthio)-1-cylopentyl-1*H*-tetrazole

S. Saglam [a], A. Disli [b], Y. Erdogdu [c], M.K. Marchewka [d,*], N. Kanagathara [e], B. Bay [b], M.T. Güllüoğlu [c]

[a] Department of Physics, Gazi University, Besevler, 06500 Ankara, Turkey
[b] Department of Chemistry, Gazi University, Besevler, 06500 Ankara, Turkey
[c] Department of Physics, Ahi Evran University, 40040 Kirsehir, Turkey
[d] Institute of Low Temperature and Structure Research, Polish Academy of Sciences, P.O. Box 937, 50-950 Wroclaw 2, Poland
[e] Department of Physics, Vel Tech Dr. RR & Dr. SR Technical University, Chennai 600062, India

HIGHLIGHTS

- 5-(Benzylthio)-1-cylopentyl-1H-tetrazole (5B1C1HT) have been synthesized.
- Complete assignment of the vibrational bands was done.
- FT-IR, ^{1}H NMR, ^{13}C-APT and LC–MS spectra for 5B1C1HT have been recorded and interpreted.
- Molecular Electrostatic Potential Maps and HOMO–LUMO of the compound were analysed.

GRAPHICAL ABSTRACT

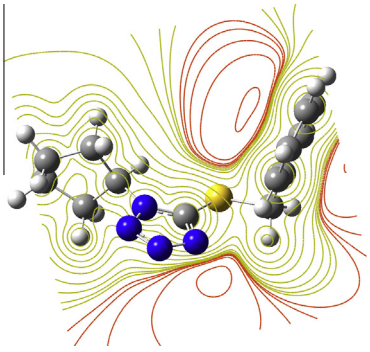

ARTICLE INFO

Article history:
Received 5 December 2013
Received in revised form 11 July 2014
Accepted 28 July 2014
Available online 7 August 2014

Keywords:
Alkyl tetrazole
Thiotetrazole
Sulfur
Alkylation
DFT
Conformational analysis

ABSTRACT

In this study, 5-(benzylthio)-1-cylopentyl-1H-tetrazole (5B1C1HT) have been synthesized. Boiling points of the obtained compound have been determined and it has been characterized by FT-IR, ^{1}H NMR, ^{13}C-APT and LC–MS spectroscopy techniques. The FT-IR, ^{1}H NMR and ^{13}C-APT spectral measurements of the 5B1C1HT compound and complete assignment of the vibrational bands observed in spectra has been discussed. The spectra were interpreted with the aid of normal coordinate analysis following full structure optimization and force field calculations based on Density Functional Theory (DFT) at 6-311++G**, cc-pVDZ and cc-pVTZ basis sets. The optimized geometry with 6-311++G** basis sets were used to determine the total energy distribution, harmonic vibrational frequencies, IR intensities.

Introduction

During the last few years tetrazoles have a great attention by the researchers and so many new synthetic methods are getting progress day by day. Due to the carboxylic acids bioisoster, tetrazoles take part in many pharmacological agents. Although having close acidity, tetrazoles are more lipophilic than corresponding carboxylate and ionized at physiological pH [1]. Because of all these properties tetrazoles have a wide range of applications and they have various biological activities. In a study, it has been show that tetrazoles have effective both on the microorganisms and DNA. In that study, either observing DNA damages or being important changes in DNA conformation have been showed [2].

* Corresponding author.
E-mail address: marchewka.mariusz578@gmail.com (M.K. Marchewka).

http://dx.doi.org/10.1016/j.saa.2014.07.071
1386-1425/

As well as synthetic organic chemistry, tetrazoles are used in polymer science, nanotechnology, biosensor, molecular identification [3–6]. As we mentioned above tetrazoles are high biological agent such as antibacterial, antifungal, antienflamatuar, antineoplastic, antiviral, antitumor agents [7]. Just a couple of decades ago especially thiotetrazoles and derivative compounds begin to used in cancer and AIDS treatment [8,9]. Furthermore, these compounds are used in synthesis of HIV-protease inhibitor for AIDS treatment and angiotensin II receptor blockers for hypertension treatment [10,11]. Tetrazole derivative compounds also effect the central nervous system [12,13]. Therefore, the researchers synthesized central nervous system stimulating compounds such as cardiazole.

In this work, we synthesized a new tetrazole derivative: 5-(benzylthio)-1-cylopentyl-1*H*-tetrazole, this compound is characterized by FT-IR, ^{1}H NMR, ^{13}C-APT and LC–MS spectroscopy techniques. In addition, we were performed the conformational analysis, structural and vibrational properties of the 5B1C1HT molecule by means of DFT calculations using the B3LYP functional with 6-311++G**, cc-pVDZ and cc-pVTZ basis sets. In the conformational analysis, the minimum energy conformational geometries were performed with the help of potential energy surface scan. The complete assignment of the bands observed in the vibrational spectra were performed taking into account the natural internal coordinates for the more stable structures by using the harmonic force field with the Pulay's Scaled Quantum Mechanics Force Field (SQMFF) methodology [14].

Experimental

All chemicals and solvents used were reagent grade (Merck or Aldrich or Sigma) and were used without additional purification. Reactions were monitored by thin layer chromatography (TLC) on precoated silica gel 60 F_{254} plates from Merck and plates were visualized by UV light. Column chromatography was performed using Merck Silica Gel 60 F_{254} (particle size: 0.63–0.200 mm; 70–230 mesh ASTM). Melting points were determined with an Electrothermal 9100 melting point apparatus and were uncorrected. IR spectrum (4000–400 cm^{-1}) was recorded using KBr disk on a Mattson 1000 FT-IR spectrometer and reported in cm^{-1} units. Fig. 1 shows the FT-IR spectrum of 5B1C1HT.

^{1}H and ^{13}C NMR spectra were recorded on a Bruker spectrometer (300 MHz for ^{1}H NMR and 75 MHz for ^{13}C NMR). Chemical shifts were reported in δ ppm units with respect to tetramethylsilane (TMS) as an internal reference in DMSO-d_6 or $CDCl_3$ and coupling constants (J) were reported in Hz units. Mass spectra measurements were recorded on a Waters ACQUITY ultra performance liquid chromatography combined with Micromass LCT Premier TM XE TOF–MS (see Figs. 2SM and 3SM in supplementary material).

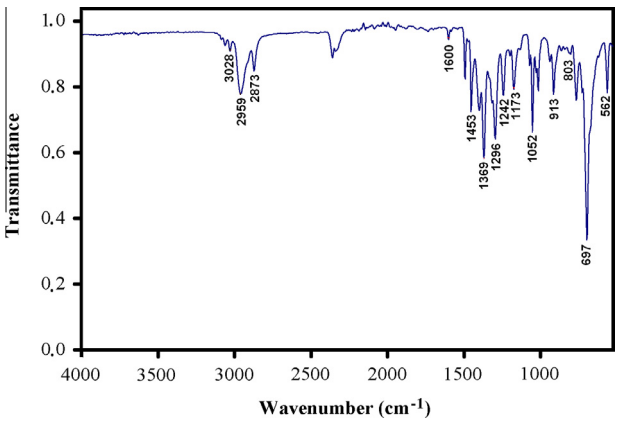

Fig. 1. FT-IR spectrum of 5B1C1HT.

Synthesis of benzyl thiocyanate

Initially, benzyl bromide (1.26 g, 0.01 mol) and potassium thiocyanate (1.16 g, 0.012 mol) in methanol (25 mL) were stirred at reflux for 2 h. Obtained KBr salt was removed by filtration at the end of the reaction and methanol was evaporated. Then (50 mL) distilled water added to the remaining slightly yellow colored benzyl thiocyanate for removing excess potassium thiocyanate. After the filtration, benzyl thiocyanate crystallized from ethanol and dried in the vacuum. Yield 85%, mp 39–41 °C, IR (KBr) υ: 3034 (aromatic —C═C—H); 2991 (aliphatic —C—H); 2153 (—SCN); 1493, 1486 (aromatic —C═C). ^{1}H NMR (300 MHz, $CDCl_3$) δ: 7.40 (s, 5H, Ar—H), 4.20 (s, 2H —S—CH2).

Synthesis of 5-(benzylthio)-1H-tetrazole

Suspension of triethylammonium chloride (0.69 g, 0.005 mol) in toluene (50 mL) was prepared in a 250-mL two-necked flask equipped with a reflux condenser. Then, sodium azide (0.33 g, 0.005 mol) was slowly added portion-wise with stirring. A solution of benzyl thiocyanate (**3**) (0.745 g, 0.005 mol) in toluene (50 mL) was slowly added, stirred for 10 min, and then heated to gentle reflux for 18 h. After cooling the reaction mixture, distilled water (20 mL) was added and the aqueous layer was separated. Then the toluene layer was washed with water (3 × 5 mL) and aqueous extracts were collected (white colored). Then the aqueous layer was cooled to room temperature and acidified to pH 3–4 using dilute HCl while stirring for 10 min. The formed solid precipitate was collected and washed with water and crystallized from ethanol and dried in the vacuum. Yield 85%, mp 136–138 °C, IR (KBr) υ: 3453 (—N—H), 3027 (aromatic —C═C—H), 2899 (aliphatic —C—H), 1635, 1543 (—C═C), 1493 (—N═N), 1457 (aromatic —C═C), ^{1}H NMR (300 MHz, $CDCl_3$) δ: 13.38–11.49 (s, 1H —N—H), 7.45–7.30 (m, 5H Ar—H), 4.52 (s, 1H —S—CH2).

Synthesis of 5-(benzylthio)-1-cylopentyl-1H-tetrazole

A mixture of (5-benzylthio)-1*H*-tetrazole (1.53 g, 0.008 mol), K_2CO_3 (2.21 g, 0.016 mol) and cyclopentyl bromide (1.78 g, 0.012 mol) in DMF (25 mL) were stirred at 100 °C for 3 h. The reaction was monitored by TLC. Reaction mixture was cooled to room temperature and work-up was made with ethyl acetate and iced-water for removing the DMF and organic was collected. After evaporation of the solvent the reaction mixture was separated by column chromatography, using a mixture of hexane–ethyl acetate (9:1) as the eluent. Yield 48%, bp 215 °C, HR–MS for $C_{13}H_{17}N_4S^{+}$ ([M−H]$^{+}$) Calc: 261.1174; Found: 261.1172. Scheme 1 is given in the supplementary material.

Computational details

The Density Functional Theory calculations were carried out by means of Gaussian 09 [15] software; invoking gradient geometry optimization [16,17]. To find the stable conformers, the potential energy surface of 5B1C1HT molecule was scanned with MMFF simulations. Conformational analysis calculation carried out with the Spartan 10 program [18] and then all conformational geometry optimized by using B3LYP/6-31G(d,p) basis set in the Gaussian 09 program package. We are determined the most stable geometry of the 5B1C1HT molecule. The optimized geometry of the most stable conformer was used in the Nuclear Magnetic Resonance,

vibrational frequency calculations and other structural and electronic properties at the DFT level. In the present work, the DFT method B3LYP with 6-311++G(d,p), cc-pVDZ and cc-pVTZ basis sets were used for the computation of all molecular properties of optimized structures. The vibrational modes were assigned on the basis of TED analysis for B3LYP/6-311++G(d,p) using SQM program [19].

NMR analysis has been performed by using Gauge Independent Atomic Orbital (GIAO) method. Theoretical chemical shifts are compared with experimental results for the identification and characterization of 5B1C1HT molecule. The ^{1}H and ^{13}C NMR chemical shifts calculations of the most stable conformer of the 5B1C1HT molecule were made by using B3LYP functional with 6-311++G(d,p) basis set. The calculations were performed in DMSO solution using IEF-PCM model. Theoretical chemical shifts are agreement with experimental ones in DMSO solution [20–24].

Results and discussion

Conformational analysis

To find stable conformers, a detailed conformational analysis was carried out for the 5B1C1HT molecule. Rotating 10 each degree intervals around the free rotation bonds, potential energy surface of the 5B1C1HT molecule was scanned by MMFF simulations. And then full geometry optimizations of these structures were performed by B3LYP/6-31G(d,p) method. The ground state conformer of the 5B1C1HT molecule have been optimized at B3LYP levels at 6-311G++(d,p) level are shown in Fig. 4SM. The optimized energies and zero point corrected optimized energies of conformers are given in Table 1. The optimized energy of other conformers is higher than those of conformer 1. As a result, the energy obtained for conformer 1 of the 5B1C1HT molecule was found to be the global minimum.

Molecular structure

The ground state conformer of the 5B1C1HT compound belongs to C_1 point group symmetry. The optimized molecular geometry of the 5B1C1HT compound is shown in Fig. 4SM. Optimized bond lengths, bond angles and dihedral angles of the molecule are predicted using B3LYP6-311++G(d,p), cc-pVDZ and cc-pVTZ levels and it is mentioned in Table 2.

Vibrational spectral analysis

Table 3 lists the results of three DFT calculations of the normal modes of vibration that were performed using the Gaussian 09 [15] program package. These results were obtained using the B3LYP functional with the 6-311++G(d,p), cc-pVDZ and cc-pVTZ basis set. The 5B1C1HT molecule has 34 atoms, which possess 96 normal modes of vibrations. All vibrations are active in Infrared spectra.

Table 1
Energetic of the nine conformers calculated at the B3LYP/6-31G(d,p) level.

Conformers	*E* (Hartree)	Δ*E* (kcal/mol)	ΔE_0 (kcal/mol)
Conformer-1	−1122.18758401	0.000	0.000
Conformer-2	−1122.18673242	0.534	0.532
Conformer-3	−1122.18536105	1.394	1.369
Conformer-4	−1122.18533564	1.410	1.333
Conformer-5	−1122.18511016	1.552	1.371
Conformer-6	−1122.18424734	2.093	1.984
Conformer-7	−1122.18373654	2.413	2.472
Conformer-8	−1122.18337209	2.642	2.652
Conformer-9	−1122.18317819	2.763	2.613

ΔE_0: zero point corrected energy.

The recorded FT-IR spectral data, calculated wavenumbers and IR intensities are given in Table 3. The total energy distributions for all fundamental vibrations were calculated using scaled quantum mechanics (SQM) method at B3LYP/6-311++G(d,p) level. The assignments were presented in terms of the percent TED of the internal motions in the modes. When relating the experimental frequencies with the calculated ones, we also considered the calculated IR intensities (Fig. 1).

$CH_{2/3}$ stretching vibrations appear between 2900 and 3000 cm^{-1} as expected [24–27]. As seen in Table 3, there are 16 Carbon–Hydrogen stretching vibrations where the five stretches of the benzyl group are predicted to range from a low value of 3012 cm^{-1} to a high of 3052 cm^{-1}, the nine stretching modes of the cyclopentyl group in the range from 2886 to 2973 cm^{-1}, and the two CH stretch vibration for the carbon attached to the sulfur atom predicted at 2939 cm^{-1} and 3002 cm^{-1}. According to the FT-Infrared spectral data, 3063 and 3086 cm^{-1} peaks are assigned to the CH stretching vibrations of the benzyl group in the FT-IR spectra. Symmetric CH stretching vibrations of the cyclopentyl group are monitored at 2873 and 2959 cm^{-1} in the Infrared spectra. 3028 cm^{-1} is determined as the asymmetric stretching vibrations of the cyclopentyl group in the FT-IR spectra. Also in the IR spectra of the compounds, the aromatic —C=C—H stretching bands are larger than those of aliphatic —C—H stretching bands.

In the 2500 cm^{-1} region, we were measured at 2146 cm^{-1} in the FT-IR spectra of benzyl thiocyanide. This peak belongs to the —CN group. In the next step synthesis, we were obtained the 5-(benzylthio)-1H-tetrazole compound. In this compound, this sharp peak was disappeared as we hoped when the aromatic tetrazole ring was obtained. This was a crucial proof of tetrazole formation in our synthesis.

In the fingerprint region, the biggest peak is the CC stretching vibrations. The stretching vibrations of Carbon–Carbon bond in the benzyl group are measured at 1173 cm^{-1}, 1585 cm^{-1} and 1600 cm^{-1} in the Infrared spectra. These vibrations are predicted at 1185 cm^{-1}, 1569 cm^{-1} and 1588 cm^{-1} in the DFT calculations (6-311+G(d,p) basis sets). These modes are mixing mode with CCH in plane bending modes. Pure CC stretching mode is calculated at 1296 cm^{-1} (6-311++G(d,p) basis set). This vibration is not experimentally observed in the FT-IR spectra.

In the fingerprint region, the most intensities peaks are experimentally appeared at 697 cm^{-1} and 1369 cm^{-1} in the FT-IR spectra. We are assigned ν_{NC} stretching τ_{CCCH} as very strong peaks. Similarly, these vibrations are calculated at 686 cm^{-1} and 1372 cm^{-1} in the DFT calculations. Infrared intensities of those are 92.89 (for 686 cm^{-1}) and 100 (for 1369 cm^{-1}) by using theoretical methods. In the present work, relative absorption intensities normalized with highest peak absorbance equal to 100.

In general, due to the band is of variable intensity, the assignment of band due to the Carbon–Sulfur stretching vibration in different compounds is difficult in the FT-IR spectra. These peaks may be found over the wide region 1035–245 cm^{-1} [28]. There are four C—S stretches for title compound. The normal modes no's are ν_{17}, ν_{18}, ν_{19} and ν_{24}. The ν_{24} mode is pure C—S stretching mode. 24th mode's is predicted at 630 cm^{-1} for B3LYP/6-311++G(d,p) level of theory. Other stretching modes are mixing with bending and stretching vibrations. CS vibrations with mixing other bending and stretching are determined in 438–468 cm^{-1} region in the DFT (6-311++G(d,p) basis sets) calculation. We are not measured these peaks in the FT-IR spectra.

Characteristic vibration peaks are generally observed in Infrared spectra at 1640–1335 and 1200–900 cm^{-1} for free tetrazole groups [28,29]. Due to the interaction of C=C, C=N, and N=N vibrations in the compound, the assignment of vibrations to the individual bonds could not be determined. The absorption bands at 1640–1335 cm^{-1} are characteristic of stretching and at 1200–900 cm^{-1}

Table 2
Optimized geometric parameters of the title compounds.

Bond lengths (Å)	6-311++G(d,p)	cc-pVDZ	cc-pVTZ	Bond angles (°)	6-311++G(d,p)	cc-pVDZ	cc-pVTZ	Dihedral angles (°)	6-311++G(d,p)	cc-pVDZ	cc-pVTZ
C_1—C_2	1.391	1.396	1.387	C_2—C_1—C_6	120.0	120.0	120.0	C_6—C_1—C_2—C_3	0.008	0.041	0.025
C_1—C_6	1.395	1.398	1.391	C_2—C_1—H_7	119.8	119.8	119.8	C_6—C_1—C_2—H_8	179.8	−179.8	−179.8
C_1—H_7	1.084	1.092	1.081	C_6—C_1—H_7	120.1	120.1	120.1	C_7—C_1—C_2—C_3	179.6	179.7	179.7
C_2—C_3	1.400	1.403	1.396	C_1—C_2—C_3	120.6	120.7	120.7	C_7—C_1—C_2—H_8	−0.160	−0.091	−0.170
C_2—H_8	1.085	1.093	1.083	C_1—C_2—H_8	119.6	119.6	119.6	C_2—C_1—C_6—C_5	0.102	0.043	0.073
C_3—C_4	1.399	1.404	1.395	C_3—C_2—H_8	119.6	119.6	119.6	C_2—C_1—C_6—H_{11}	179.8	179.8	179.8
C_3—C_{12}	1.500	1.505	1.500	C_2—C_3—C_4	118.9	118.9	118.9	H_7—C_1—C_6—C_5	179.5	−179.6	−179.6
C_4—C_5	1.394	1.397	1.390	C_2—C_3—C_{12}	120.4	120.3	120.4	H_7—C_1—C_6—H_{11}	0.193	0.126	0.167
C_4—H_9	1.083	1.091	1.081	C_4—C_3—C_{12}	120.5	120.6	120.6	C_1—C_2—C_3—C_4	−0.16	−0.121	−0.127
C_5—C_6	1.393	1.398	1.389	C_3—C_4—C_5	120.3	120.2	120.3	C_1—C_2—C_3—C_{12}	−179.4	−179.5	−179.4
C_5—H_{10}	1.084	1.092	1.081	C_3—C_4—H_9	119.3	119.2	119.3	H_8—C_2—C_3—C_4	179.6	179.7	179.7
C_6—H_{11}	1.084	1.092	1.081	C_5—C_4—H_9	120.3	120.5	120.3	H_8—C_2—C_3—C_{12}	0.374	0.317	0.471
C_{12}—H_{13}	1.091	1.099	1.088	C_4—C_5—C_6	120.2	120.3	120.2	C_2—C_3—C_4—C_5	0.219	0.117	0.133
C_{12}—H_{14}	1.088	1.096	1.085	C_4—C_5—H_{10}	119.6	119.5	119.6	C_2—C_3—C_4—H_9	179.6	179.5	179.5
C_{12}—S_{15}	1.863	1.868	1.857	C_6—C_5—H_{10}	120.0	120.0	120.0	C_{12}—C_3—C_4—C_5	179.5	179.5	179.4
S_{15}—C_{16}	1.755	1.759	1.751	C_1—C_6—C_5	119.7	119.6	119.7	C_{12}—C_3—C_4—H_9	−1.071	−1.084	−1.196
C_{16}—N_{17}	1.322	1.327	1.320	C_1—C_6—H_{11}	120.0	120.1	120.1	C_2—C_3—C_{12}—H_{13}	33.37	28.81	33.49
C_{16}—N_{20}	1.352	1.355	1.349	C_5—C_6—H_{11}	120.1	120.1	120.1	C_2—C_3—C_{12}—H_{14}	156.0	151.9	156.0
N_{17}—N_{18}	1.356	1.359	1.355	C_3—C_{12}—H_{13}	111.6	111.5	111.4	C_2—C_3—C_{12}—S_{15}	−82.35	−87.11	−82.31
N_{18}—N_{19}	1.287	1.289	1.283	C_3—C_{12}—H_{14}	112.4	112.5	112.3	C_4—C3—C_{12}—H_{13}	−145.9	−150.5	−145.7
N_{19}—N_{20}	1.356	1.358	1.353	C_3—C_{12}—S_{15}	114.4	114.5	114.6	C_4—C_3—C_{12}—H_{14}	−23.25	−27.47	−23.22
N_{20}—C_{21}	1.468	1.467	1.463	H_{13}—C_{12}—H_{14}	108.8	109.1	108.8	C_4—C_3—C_{12}—S_{15}	98.34	93.48	98.40
C_{21}—C_{22}	1.554	1.556	1.549	H_{13}—C_{12}—S_{15}	102.4	102.5	102.4	C_3—C_4—C_5—C_6	−0.111	−0.034	−0.036
C_{21}—C_{23}	1.557	1.556	1.555	H_{14}—C_{12}—S_{15}	106.4	105.8	106.3	C_3—C_4—C_5—H_{10}	−179.9	−179.8	−179.9
C_{21}—H_{24}	1.090	1.098	1.087	C_{12}—S_{15}—C_{16}	100.1	99.93	100.5	H_9—C_4—C_5—C_6	179.5	−179.4	−179.4
C_{22}—C_{25}	1.538	1.538	1.533	S_{15}—C_{16}—N_{17}	127.3	127.7	127.5	H_9—C_4—C_5—H_{10}	0.661	0.747	0.699
C_{22}—H_{26}	1.092	1.100	1.090	S_{15}—C_{16}—N_{20}	124.0	123.7	123.8	C_4—C_5—C_6—C_1	−0.051	−0.047	−0.067
C_{22}—H_{27}	1.091	1.100	1.089	N_{17}—C_{16}—N_{20}	108.5	108.5	108.5	C_4—C_5—C_6—H_{11}	−179.8	−179.8	−179.8
C_{23}—C_{28}	1.538	1.537	1.536	C_{16}—N_{17}—N_{18}	105.8	105.7	105.7	H_{10}—C_5—C_6—C_1	179.7	179.7	179.8
C_{23}—H_{29}	1.089	1.098	1.087	N_{17}—N_{18}—N_{19}	111.2	111.3	111.1	H_{10}—C_5—C_6—H_{11}	0.006	−0.009	0.032
C_{23}—H_{30}	1.093	1.102	1.090	N_{18}—N_{19}—N_{20}	106.8	106.8	106.9	C_3—C_{12}—S_{15}—C_{16}	−80.36	−86.19	−82.87
C_{25}—C_{28}	1.536	1.536	1.533	C_{16}—N_{20}—N_{19}	107.5	107.5	107.5	H_{13}—C_{12}—S_{15}—C_{16}	158.6	152.7	156.1
C_{25}—H_{31}	1.096	1.104	1.093	C_{16}—N_{20}—C_{21}	130.8	130.9	130.8	H_{14}—C_{12}—S_{15}—C_{16}	44.44	38.43	41.98
C_{25}—H_{32}	1.092	1.100	1.089	N_{19}—N_{20}—C_{21}	121.6	121.4	121.6	C_{12}—S_{15}—C_{16}—N_{17}	−20.08	−10.34	−15.82
C_{28}—H_{33}	1.092	1.100	1.089	N_{20}—C_{21}—C_{22}	112.2	111.9	112.3	C_{12}—S_{15}—C_{16}—N_{20}	161.6	171.3	165.9
C_{28}—H_{34}	1.094	1.102	1.091	N_{20}—C_{21}—C_{23}	112.6	112.4	112.9	S_{15}—C_{16}—N_{17}—N_{18}	−178.3	−178.3	−178.3
				N_{20}—C_{21}—H_{24}	104.7	104.8	104.8	N_{20}—C_{16}—N_{17}—N_{18}	0.073	0.214	0.136
				C_{22}—C_{21}—C_{23}	106.0	105.8	105.9	S_{15}—C_{16}—N_{20}—N_{19}	178.0	178.0	178.0
				C_{22}—C_{21}—H_{24}	111.0	111.4	110.8	S_{15}—C_{16}—N_{20}—C_{21}	−1.99	−0.359	−1.019
				C_{23}—C_{21}—H_{24}	110.2	110.4	110.0	N_{17}—C_{16}—N_{20}—N_{19}	−0.490	−0.576	−0.525
				C_{21}—C_{22}—C_{25}	104.9	105.1	104.7	N_{17}—C_{16}—N_{20}—C_{21}	179.4	−178.9	−179.5
				C_{21}—C_{22}—H_{26}	108.6	108.2	108.5	C_{16}—N_{17}—N_{18}—N_{19}	0.401	0.249	0.330
				C_{21}—C_{22}—H_{27}	112.0	112.2	112.1	N_{17}—N_{18}—N_{19}—N_{20}	−0.701	−0.603	−0.652
				C_{25}—C_{22}—H_{26}	109.7	109.7	109.6	N_{18}—N_{19}—N_{20}—C_{16}	0.726	0.718	0.718
				C_{25}—C_{22}—H_{27}	113.6	113.7	113.7	N_{18}—N_{19}—N_{20}—C_{21}	−179.2	179.2	179.8
				H_{26}—C_{22}—H_{27}	107.7	107.6	107.7	C_{16}—N_{20}—C_{21}—C_{22}	112.7	109.6	110.9
				C_{21}—C_{23}—C_{28}	105.4	105.3	105.6	C_{16}—N_{20}—C_{21}—C_{23}	−127.6	−131.3	−129.2
				C_{21}—C_{23}—H_{29}	111.6	111.6	111.4	C_{16}—N_{20}—C_{21}—H_{24}	−7.869	−11.30	−9.436
				C_{21}—C_{23}—H_{30}	108.5	108.5	108.7	N_{19}—N_{20}—C_{21}—C_{22}	−67.32	−68.53	−67.95
				C_{28}—C_{23}—H_{29}	113.4	113.6	113.1	N_{19}—N_{20}—C_{21}—C_{23}	52.32	50.46	51.81
				C_{28}—C_{23}—H_{30}	110.1	109.9	110.2	N_{19}—N_{20}—C_{21}—H_{24}	172.1	170.5	171.6
				H_{29}—C_{23}—H_{30}	107.5	107.6	107.5	N_{20}—C_{21}—C_{22}—C_{25}	138.6	136.5	141.6
				C_{22}—C_{25}—C_{28}	103.3	103.2	103.1	N_{20}—C_{21}—C_{22}—H_{26}	21.26	19.36	24.51
				C_{22}—C_{25}—H_{31}	110.4	110.4	110.4	N_{20}—C_{21}—C_{22}—H_{27}	−97.6	−99.3	−94.45
				C_{22}—C_{25}—H_{32}	112.2	112.3	112.3	C_{23}—C_{21}—C_{22}—C_{25}	15.18	13.70	17.90
				C_{28}—C_{25}—H_{31}	110.0	109.9	110.1	C_{23}—C_{21}—C_{22}—H_{26}	−102.6	−103.4	−99.22
				C_{28}—C_{25}—H_{32}	113.3	113.5	113.3	C_{23}—C_{21}—C_{22}—H_{27}	138.9	137.7	141.8
				H_{31}—C_{25}—H_{32}	107.3	107.3	107.3	H_{24}—C_{21}—C_{22}—C_{25}	−104.5	−106.3	−101.4
				C_{23}—C_{28}—C_{25}	103.4	103.1	103.7	H_{24}—C_{21}—C_{22}—H_{26}	138.0	136.4	141.3
				C_{23}—C_{28}—H_{33}	112.5	112.7	112.5	H_{24}—C_{21}—C_{22}—H_{27}	19.18	17.70	22.43
				C_{23}—C_{28}—H_{34}	109.9	109.7	109.8	N_{20}—C_{21}—C_{23}—C_{28}	−112.9	−110.2	−115.9
				C_{25}—C_{28}—H_{33}	113.2	113.4	113.2	N_{20}—C_{21}—C_{23}—H_{29}	10.70	13.52	7.246
				C_{25}—C_{28}—H_{34}	109.8	109.8	109.6	N_{20}—C_{21}—C_{23}—H_{30}	129.0	131.9	125.6
				H_{33}—C_{28}—H_{34}	107.7	107.9	107.6	C_{22}—C_{21}—C_{23}—C_{28}	10.20	12.24	7.361
								C_{22}—C_{21}—C_{23}—H_{29}	133.8	136.0	130.5
								C_{22}—C_{21}—C_{23}—H_{30}	−107.7	−105.5	−111.0
								H_{24}—C_{21}—C_{23}—C_{28}	130.5	132.9	127.2
								H_{24}—C_{21}—C_{23}—H_{29}	−105.8	−103.2	−109.5
								H_{24}—C_{21}—C_{23}—H_{30}	12.52	15.22	8.864
								C_{21}—C_{22}—C_{25}—C_{28}	−34.87	−34.47	−36.42
								C_{21}—C_{22}—C_{25}—H_{31}	82.81	83.03	81.27
								C_{21}—C_{22}—C_{25}—H_{32}	−157.3	−157.1	−158.8
								H_{26}—C_{22}—C_{25}—C_{28}	81.69	81.75	79.92
								H_{26}—C_{22}—C_{25}—H_{31}	−160.6	−160.7	−162.3

Table 2 (*continued*)

Bond lengths (Å)	6-311++G(d,p)	cc-pVDZ	cc-pVTZ	Bond angles (°)	6-311++G(d,p)	cc-pVDZ	cc-pVTZ	Dihedral angles (°)	6-311++G(d,p)	cc-pVDZ	cc-pVTZ
								H_{26}—C_{22}—C_{25}—H_{32}	−40.91	−40.91	−42.51
								H_{27}—C_{22}—C_{25}—C_{28}	−157.5	−157.6	−159.2
								H_{27}—C_{22}—C_{25}—H_{31}	−39.90	−40.09	−41.56
								H_{27}—C_{22}—C_{25}—H_{32}	79.89	79.77	78.30
								C_{21}—C_{23}—C_{28}—C_{25}	−31.73	−33.54	−29.82
								C_{21}—C_{23}—C_{28}—H_{33}	−154.3	−156.2	−152.6
								C_{21}—C_{23}—C_{28}—H_{34}	85.56	83.43	87.38
								H_{29}—C_{23}—C_{28}—C_{25}	−154.2	−156.0	−152.0
								H_{29}—C_{23}—C_{28}—H_{33}	83.22	81.20	85.19
								H_{29}—C_{23}—C_{28}—H_{34}	−36.91	−39.08	−34.80
								H_{30}—C_{23}—C_{28}—C_{25}	85.20	83.19	87.52
								H_{30}—C_{23}—C_{28}—H_{33}	−37.36	−39.53	−35.27
								H_{30}—C_{23}—C_{28}—H_{34}	−157.5	−159.8	−155.2
								C_{22}—C_{25}—C_{28}—C_{23}	41.33	42.16	41.10
								C_{22}—C_{25}—C_{28}—H_{33}	163.4	164.4	163.4
								C_{22}—C_{25}—C_{28}—H_{34}	−76.03	−74.74	−76.22
								H_{31}—C_{25}—C_{28}—C_{23}	−76.62	−75.69	−76.83
								H_{31}—C_{25}—C_{28}—H_{33}	45.47	46.57	45.48
								H_{31}—C_{25}—C_{28}—H_{34}	166.0	167.3	165.8
								H_{32}—C_{25}—C_{28}—C_{23}	163.1	164.0	162.8
								H_{32}—C_{25}—C_{28}—H_{33}	−74.77	−73.64	−74.78
								H_{32}—C_{25}—C_{28}—H_{34}	45.75	47.17	45.56

of skeletal vibrations of a cycle. In the present work, 1369 cm^{-1} peak is belongs to the —C═N double bonds stretching of this group in the FT-IR spectra. The skeletal vibration of the tetrazole group is appeared at 1072 cm^{-1} in the FT-IR spectra. This peak is predicted at 1066 cm^{-1} by using the DFT computations.

The obtained TED results show that the NN stretching vibrations are calculated at 1284, 1275, 1032 and 978 cm^{-1} by DFT computations. According to the TED results, 1032 and 1284 pure NN stretching modes. Other of them are mixing modes with tetrazole group vibrations. In the experimental data, only one mode is monitored in the FT-IR spectra. This peak is determined at 1296 cm^{-1}. Other modes is not determined in the experimental spectra.

The CH_2 scissoring vibrations are measured at 1453 cm^{-1} in the Infrared spectra. These vibrations are predicted at 1438–1464 cm^{-1} region. Other CH_2 scissoring vibration is obtained at 1400 cm^{-1} in the FT-IR spectra. This peak possess to the scissoring vibrations of the S—CH_2 group. The predicted vibrational frequencies have been compared with the experimental FT-IR spectra. The observed and the calculated frequencies are found to be in good agreement.

NMR spectra

The measured ^{13}C and ^{1}H NMR spectra are shown in Figs. 2SM and 3SM. The computed and observed ^{13}C NMR and ^{1}H NMR chemical shift values are tabulated in Table 4. The calculated values of ^{13}C and ^{1}H chemical shifts by B3LYP/6-311++G(d, p) level of theory in DMSO environment are summarized.

The ^{1}H NMR spectra of the title compound, the lowest NMR signals belongs to the methylene group of cyclopentyl ring. These signals were showed in the range 2.29–1.67 ppm. These peaks are appeared in the region 1.60–2.40 ppm by DFT computations. The ^{1}H NMR spectra of the cyclopentyl thiotetrazole compounds showed the singlet peaks belong to protons of the methylene groups between aromatic benzene ring and sulfur atom at the 4.42 ppm. These chemical shifts are predicted at 4.13 ppm (H_{13}) and 5.17 ppm (H_{14}) by means of DFT computations.

Multiple peaks were showed in the range 5.23–4.56 ppm for the —CH group protons of the cyclopentyl bounded tetrazole ring. This signal of H_{24} proton is calculated at 4.60 ppm by DFT. In the pentyl group, it has the larger ^{1}H NMR signals in both experimental and theoretical spectra The ^{1}H NMR signals of the phenyl group for the aromatic protons in the range 7.38–7.24 ppm. These signals are observed at 7.24 ppm (H_{10}), 7.29 ppm (H_{11}), 7.35 ppm (H_7), 7.37 ppm (H_8) and 7.38 ppm (H_9) by experimental methods. We are calculated at 7.38 ppm (H_{10}), 7.48 ppm (H_{11}), 7.60 ppm (H_7), 7.71 ppm (H_8) and 8.02 ppm (H_9) in the theoretical method. Moreover, at the compound 5-(benzylthio)-1*H*-tetrazole we monitored an N—H signal about 12.43 ppm belongs to the tetrazole ring as weak and broad. This data also prove the tetrazole formation.

In the previously work [30,31], it note that the range of ^{13}C NMR chemical shifts for a typical organic molecule usually is bigger than 100 ppm, the accuracy ensures reliable interpretation of spectroscopic parameters. In the present paper, ^{13}C NMR chemical shifts of the pentyl and tetrazole group for the title compound are larger than 100 ppm. These signals are observed in the region 127.15–163.0 ppm in the experimental spectra. We are performed at the 132.7 (C_5), 132.9 (C_6), 133.8 (C_1), 134.9 (C_2), 135.3 (C_4), 146.2 (C_3) and 163.3 (C_{16}) by using the theoretical calculations. As seen in Table 4, the observed and the calculated ^{13}C NMR signals are found to be in good agreement. 163.3 ppm signal posses to the tetrazole group and are higher signal in the ^{13}C NMR spectra. Other peaks belong to the carbon atoms of the phenyl group.

According to ^{13}C NMR signal of the phenyl and tetrazole group, the chemical shifts of obtained and calculated for the ^{1}H atoms of cyclopentyl group are lower than those. All signals are smaller than 100 ppm. The bigger signal is that of C_{21} atom. This peak observed experimentally at 65.19 ppm and theoretically at 65.23 ppm. Other signals are calculated in the region 30.09–44.19 ppm and measured in the 24.27–37.86 ppm. According to the NMR spectra, the observed and the calculated NMR signals are found to be in good agreement.

Molecular Electrostatic Potential Maps (MEP)

MEP that is occurred by the nuclei and the electrons is a very useful property for analyzing and predicting molecular reactive behavior. MEP mapping is very useful in the investigation of the molecular structure with its physiochemical property relationship. The potential has been particularly useful as an indicator of the sites or regions of a molecule to which an approaching electrophile is initially attracted, and it has also been applied successfully to the study of interactions that involve a certain optimum relative orientation of the reactants.

Table 3
Calculated (B3LYP) vibrational wavenumbers (cm^{-1}), measured FT-IR bands and assignments for the title compound.

	6-311++G,p		cc-pVDZ	cc-pVTZ	Exp. IR	TED[c] (%)
	Freq[a]	I_{IR}[b]	Freq[a]	Freq[a]		
ν_1	0	0.838	13	12		$\tau_{NCSC}(42\%) + \tau_{CCNC}(29\%)$
ν_2	22	0.087	26	24		$\tau_{NCSC}(28\%) + \tau_{CSCH}(13\%) + \tau_{HCCC}(10\%) + \tau_{CSCC}(10\%) + \tau_{CCNN}(10\%)$
ν_3	27	2.449	28	31		$\tau_{CSCH}(19\%) + \tau_{HCCC}(18\%) + \tau_{CSCC}(16\%) + \tau_{NCSC}(12\%)$
ν_4	31	0.313	36	44		$\tau_{HCCN}(35\%) + \tau_{CCCN}(26\%) + \tau_{CCCH}(10\%)$
ν_5	51	2.906	55	52		$\tau_{SCCC}(47\%) + \tau_{CSCC}(17\%) + \tau_{CSCH}(10\%)$
ν_6	107	1.637	106	109		$\tau_{CCCC}(25\%) + \delta_{SCC}(22\%) + \tau_{CCCH}(22\%)$
ν_7	115	4.453	115	116		$\tau_{CNCN}(18\%) + \tau_{CNNN}(15\%) + \tau_{CNCS}(14\%) + \tau_{NCSC}(13\%)$
ν_8	118	4.014	123	120		$\delta_{NCS}(40\%) + \delta_{CNC}(14\%) + \delta_{CNN}(10\%) + \delta_{CSC}(10\%)$
ν_9	159	2.994	163	161		$\delta_{CSC}(44\%) + \delta_{CNC}(10\%) + \delta_{CNN}(10\%)$
ν_{10}	221	0.672	228	226		$\tau_{NNCS}(36\%) + \tau_{CNCS}(11\%)$
ν_{11}	245	3.267	245	249		$\tau_{HCCC}(33\%) + \tau_{CCCC}(16\%)$
ν_{12}	261	2.266	270	259		$\tau_{HCCC}(22\%) + \tau_{CCCC}(10\%)$
ν_{13}	288	1.170	287	289		$\delta_{SCC}(15\%) + \tau_{CCCC}(10\%) +$
ν_{14}	328	3.332	335	331		$\delta_{CCC}(66\%)$
ν_{15}	400	0.014	404	403		$\tau_{CCCC}(63\%) + \tau_{CCCH}(33\%) +$
ν_{16}	405	0.823	411	406		$\delta_{CCN}(26\%) + \tau_{HCCN}(25\%) + \tau_{CCCN}(11\%)$
ν_{17}	438	1.953	442	439		$\nu_{CS}(14\%) + \delta_{NCS}(11\%) + \nu_{CN}(10\%)$
ν_{18}	465	1.928	467	467		$\nu_{CS}(34\%) + \delta_{NCS}(14\%) + \delta_{CSC}(11\%)$
ν_{19}	468	9.772	473	470		$\nu_{SC}(20\%) + \tau_{CCCH}(11\%) + \tau_{CCCC}(10\%)$
ν_{20}	524	1.107	523	525		$\delta_{CCC}(27\%) + \tau_{HCCC}(22\%) + \delta_{HCC}(10\%)$
ν_{21}	552	15.08	552	554	562	$\delta_{CCC}(34\%) + \delta_{SCC}(10\%)$
ν_{22}	614	1.576	612	612		$\delta_{CCC}(57\%) + \delta_{CCH}(18\%)$
ν_{23}	615	0.746	619	615	620	$\delta_{CCC}(16\%) + \tau_{CCCH}(10\%)$
ν_{24}	630	81.45	633	633		$\nu_{SC}(62\%)$
ν_{25}	664	13.83	667	670		$\tau_{NNCN}(19\%) + \nu_{CN}(16\%)$
ν_{26}	677	4.017	688	693		$\tau_{NNCN}(22\%) + \tau_{CNNN}(13\%) + \tau_{NCSC}(10\%)$
ν_{27}	686	92.89	695	697	697	$\tau_{CCCH}(55\%) + \tau_{CCCC}(33\%)$
ν_{28}	700	0.590	704	708	728	$\tau_{NNNC}(43\%) + \tau_{NNNN}(26\%) + \tau_{NNCN}(16\%)$
ν_{29}	752	29.11	761	759	766	$\tau_{CCCH}(53\%) + \tau_{CCCC}(10\%)$
ν_{30}	793	8.060	797	794		$\nu_{CC}(53\%) + \delta_{CCC}(15\%)$
ν_{31}	803	12.38	804	804	803	$\nu_{CC}(14\%) + \tau_{HCCH}(13\%) + \tau_{HCCC}(12\%)$
ν_{32}	829	1.234	838	835	814	$\tau_{CCCH}(81\%) + \tau_{HCCH}(17\%)$
ν_{33}	836	2.743	843	837	840	$\nu_{CC}(27\%) + \tau_{HCCC}(20\%) + \delta_{HCC}(19\%)$
ν_{34}	856	2.181	850	853		$\tau_{HCCC}(26\%) + \delta_{HCC}(14\%) + \tau_{CSCH}(12\%) + \tau_{SCCC}(10\%) + \delta_{HCS}(10\%)$
ν_{35}	875	13.41	885	873	863	$\nu_{CC}(77\%)$
ν_{36}	880	5.070	890	879		$\nu_{CC}(60\%)$
ν_{37}	893	4.914	898	895		$\nu_{CC}(40\%) + \delta_{CCH}(12\%)$
ν_{38}	905	4.529	914	914		$\tau_{CCCH}(55\%) + \tau_{HCCH}(32\%)$
ν_{39}	919	6.101	921	921	913	$\delta_{CCH}(18\%) + \tau_{HCCH}(15\%) + \nu_{CC}(14\%)$
ν_{40}	955	0.789	961	960	941	$\tau_{HCCH}(54\%) + \tau_{CCCH}(33\%)$
ν_{41}	971	0.393	982	974		$\tau_{HCCH}(65\%) + \tau_{HCCC}(16\%)$
ν_{42}	978	14.59	985	979		$\nu_{NN}(38\%) + \delta_{NNC}(17\%) + \nu_{NC}(14\%)$
ν_{43}	984	0.256	988	988		$\nu_{CC}(39\%) + \delta_{CCC}(39\%)$
ν_{44}	992	2.317	995	992		$\nu_{CC}(38\%) + \tau_{HCCH}(10\%)$
ν_{45}	1008	10.71	1012	1009	1014	$\nu_{CC}(49\%) + \tau_{HCCH}(10\%)$
ν_{46}	1016	7.746	1020	1018	1029	$\delta_{CCH}(26\%) + \nu_{CC}(24\%) + \nu_{CC}(23\%) + \delta_{CCC}(14\%)$
ν_{47}	1032	34.82	1043	1026		$\nu_{NN}(71\%)$
ν_{48}	1056	2.758	1064	1052	1052	$\nu_{CC}(23\%) + \nu_{NN}(11\%)$
ν_{49}	1065	19.30	1066	1061		$\nu_{CC}(29\%) + \delta_{HCC}(18\%) + \delta_{NNN}(14\%)$
ν_{50}	1066	20.62	1074	1066	1072	$\delta_{NNN}(23\%) + \nu_{CC}(16\%) + \nu_{NN}(10\%)$
ν_{51}	1126	65.47	1125	1128		$\delta_{HCC}(15\%) + \delta_{NNN}(10\%)$
ν_{52}	1143	0.218	1135	1141	1133	$\delta_{CCH}(59\%) + \nu_{CC}(17\%)$
ν_{53}	1148	0.387	1138	1146		$\delta_{HCC}(39\%) + \delta_{HCS}(26\%)$
ν_{54}	1152	9.031	1151	1153		$\delta_{HCC}(20\%) + \tau_{HCCH}(17\%)$
ν_{55}	1166	2.724	1160	1167		$\delta_{CCH}(76\%) + \nu_{CC}(16\%)$
ν_{56}	1185	7.565	1187	1184	1173	$\nu_{CC}(64\%) + \delta_{HCC}(14\%)$
ν_{57}	1192	3.791	1189	1195		$\delta_{CCH}(25\%) + \tau_{CCCH}(11\%)$
ν_{58}	1198	27.59	1203	1197	1199	$\nu_{NC}(27\%) + \delta_{NNC}(10\%)$
ν_{59}	1219	6.295	1218	1222		$\delta_{CCH}(39\%) + \tau_{CCCH}(10\%)$
ν_{60}	1234	56.83	1220	1227		$\delta_{HCS}(37\%) + \delta_{HCC}(22\%) + \tau_{HCCC}(33\%)$
ν_{61}	1264	0.034	1254	1268	1242	$\delta_{CCH}(28\%) + \tau_{HCCH}(14\%)$
ν_{62}	1275	5.599	1272	1277		$\nu_{NN}(26\%) + \delta_{HCC}(23\%)$
ν_{63}	1284	24.90	1292	1285	1296	$\nu_{NN}(40\%)$
ν_{64}	1296	0.731	1301	1293		$\nu_{CC}(67\%)$
ν_{65}	1297	15.99	1304	1298		$\delta_{HCC}(26\%) + \tau_{HCCC}(25\%)$
ν_{66}	1303	3.323	1306	1304		$\delta_{CCH}(36\%) + \tau_{HCCH}(28\%) + \tau_{HCCC}(12\%)$
ν_{67}	1309	1.114	1307	1310		$\delta_{HCC}(42\%)$
ν_{68}	1319	2.472	1319	1324	1316	$\delta_{CCH}(87\%)$
ν_{69}	1345	42.75	1346	1344		$\nu_{NC}(31\%) + \tau_{HCCH}(13\%) + \tau_{CCCH}(10\%)$
ν_{70}	1372	100	1389	1368	1369	$\nu_{NC}(62\%) + \tau_{NNC}(12\%) + \nu_{NN}(10\%)$
ν_{71}	1413	62.41	1395	1411		$\nu_{NC}(25\%) + \tau_{HCCH}(11\%)$
ν_{72}	1417	58.70	1406	1415	1400	$\delta_{HCH}(35\%) + \tau_{CSCH}(19\%) + \tau_{HCCC}(16\%) + \delta_{HCC}(12\%)$
ν_{73}	1436	10.19	1414	1438		$\delta_{CCH}(54\%) + \nu_{CC}(29\%)$

Table 3 (*continued*)

	6-311++G,p		cc-pVDZ	cc-pVTZ	Exp. IR	TED[c] (%)
	Freq[a]	I_{IR}[b]	Freq[a]	Freq[a]		
ν_{74}	1438	2.686	1420	1441		$\delta_{HCH}(24\%) + \tau_{HCCH}(23\%) + \tau_{CCCH}(12\%)$
ν_{75}	1442	13.66	1424	1442		$\delta_{HCH}(27\%) + \tau_{HCCH}(25\%)$
ν_{76}	1446	11.68	1438	1447		$\delta_{HCH}(29\%) + \tau_{HCCH}(29\%)$
ν_{77}	1464	11.23	1443	1464	1453	$\delta_{HCH}(34\%) + \tau_{HCCH}(27\%)$
ν_{78}	1476	14.95	1479	1481	1473	$\delta_{CCH}(62\%) + \nu_{CC}(33\%)$
ν_{79}	1569	1.351	1586	1570	1585	$\nu_{CC}(70\%) + \delta_{CCH}(12\%)$
ν_{80}	1588	2.502	1605	1589	1600	$\nu_{CC}(67\%) + \delta_{CCH}(16\%)$
ν_{81}	2886	58.11	2936	2918	2873	$\nu_{HC}(96\%)$
ν_{82}	2905	36.31	2955	2937	2959	$\nu_{HC}(100\%)$
ν_{83}	2909	34.59	2957	2943		$\nu_{HC}(97\%)$
ν_{84}	2917	26.44	2968	2949		$\nu_{HC}(99\%)$
ν_{85}	2939	16.42	2989	2969		$\nu_{HC}(100\%)$
ν_{86}	2942	65.21	2996	2974		$\nu_{HC}(95\%)$
ν_{87}	2949	18.03	3001	2979		$\nu_{HC}(97\%)$
ν_{88}	2951	48.50	3007	2983		$\nu_{HC}(99\%)$
ν_{89}	2965	31.16	3020	2996		$\nu_{HC}(95\%)$
ν_{90}	2973	39.77	3029	3007	3028	$\nu_{HC}(91\%)$
ν_{91}	3002	0.080	3058	3032		$\nu_{HC}(100\%)$
ν_{92}	3012	11.09	3068	3046	3063	$\nu_{HC}(98\%)$
ν_{93}	3023	2.330	3079	3057	3086	$\nu_{HC}(99\%)$
ν_{94}	3033	32.13	3090	3067		$\nu_{HC}(100\%)$
ν_{95}	3043	25.45	3101	3077		$\nu_{HC}(9(6\%)$
ν_{96}	3050	14.79	3108	3084		$\nu_{HC}(98\%)$

[a] Obtained from the wave numbers calculated at 0.967 for 6-311++G(d,p)), 0.970 for cc-pVDZ, 0.965 for cc-pVTZ. ν: stretching, δ: bending, τ: torsion.
[b] Relative absorption intensities normalized with highest peak absorption equal to 100.
[c] Total energy distribution calculated B3LYP/6-311++G(d,p) level of theory. Only contributions 10% are listed.

Table 4
The observed and predicted ^{1}H and ^{13}C NMR isotropic chemical shifts (with respect to TMS, all values in ppm) f.

Atom numbering	Theoretical	Experimental
C_{28}	30.09	24.27
C_{25}	31.71	24.27
C_{23}	37.73	32.79
C_{22}	39.27	32.79
C_{12}	44.19	37.86
C_{21}	62.37	65.19
C_5	132.7	127.5
C_6	132.9	127.5
C_1	133.8	128.8
C_2	134.9	128.8
C_4	135.3	129.0
C_3	146.2	136.8
C_{16}	163.3	163.0
H_{31}	1.60	1.67
H_{29}	1.71	1.67
H_{33}	1.75	1.67
H_{26}	1.75	1.67
H_{34}	1.95	2.20
H_{32}	1.98	2.20
H_{30}	2.01	2.20
H_{27}	2.40	2.29
H_{24}	4.60	5.23–4.56
H_{13}	4.13	4.42
H_{14}	5.17	4.42
H_{10}	7.38	7.24
H_{11}	7.48	7.29
H_7	7.60	7.35
H_8	7.71	7.37
H_9	8.02	7.38

Electronic properties

The evolvement of the electronic structure can be by calculating the highest occupied molecular orbital (HOMO), the lowest unoccupied molecular orbital (LUMO) as well as the energy gap (E_{GAP}) between HOMO and LUMO. Both HOMO and LUMO are the main orbital taking part in chemical reaction (see HOMO–LUMO plot in supplementary materials). The HOMO energy characterizes the ability of electron giving, the LUMO characterizes the ability of electron accepting, and the gap between HOMO and LUMO characterizes the molecular chemical stability. The energy gap between the HOMO's and LUMO's is the most important parameter in determining molecular electrical transport properties because it is a measure of electron conductivity. The values of LUMO and HOMO and their energy gap consider the chemical activity of the molecule. The decrease in the HOMO and LUMO energy gap shows the eventual charge transfer interaction taking place within the molecule which is responsible for the activity of the molecule.

Conclusion

Firstly, we have been synthesized the 5-(benzylthio)-1-cylopentyl-1H-tetrazole (5B1C1HT) compound. The FT-IR, ^{1}H NMR, ^{13}C-APT and LC–MS spectra for 5B1C1HT have been recorded and interpreted. Theoretical conformational, structural, vibrational and Nuclear Magnetic Resonance spectral analyses of 5B1C1HT molecule were performed by Gaussian 09 and Spartan 10 software. The NMR and FT-IR spectral experimental results were compared with the theoretical values. The NMR chemical shifts and the peaks of FT-IR spectra experimentally showed good agreement with the theoretical values. In addition, we plotted the Molecular Electrostatic Potential Maps and HOMO–LUMO of the title compound.

Acknowledgements

One of the Authors (Y. Erdogdu) thanks to Ahi Evran University Research Fund for its financial support. Project Numbers: FEN.4003.12.007. Computing resources used in this work were provided by the National Center for High Performance Computing of Ahi Evran University in Turkey (AHILAB).

Appendix A. Supplementary data

Supplementary data associated with this article can be found, in the online version, at http://dx.doi.org/10.1016/j.saa.2014.07.071.

References

[1] R. Herr, J. Bioorg. Med. Chem. 10 (2002) 3379–3393.
[2] G.D. Celik, A. Disli, Y. Oner, L. Acık, Med. Chem. Res. 3 (2012) 1470–1479.
[3] Z.P. Demko, K.B. Sharpless, J. Org. Chem. 66 (2001) 7945–7949.
[4] F. Himo, Z.P. Demko, L. Noodleman, K.P. Sharpless, J. Am. Chem. Soc. 125 (2003) 9983–9987.
[5] A.S. Gundusola, K.L. Chandra, E.M. Perchellet, A.M. Waters, J.P.H. Perchellet, S. Rayat, Bioorg. Med. Chem. Lett. 20 (2010) 3920–3924.
[6] H. Zhao, Z.R. Qu, H.Y. Ye, R.G. Xiong, Chem. Soc. Rev. 37 (2008) 84–100.
[7] O.A. Shemyakina, A.G. Mal'kina, A.I. Albanov, B.A. Trofimov, Chem. Heterocycl. Compd. 47 (2011) 464–469.
[8] Y. Tamura, F. Watanabe, T. Nakatani, K. Yasui, M. Fuji, T. Komurasaki, H. Tsuzuki, R. Maekawa, T. Yoshioki, K. Kawada, K. Sugita, M. Ohtani, J. Med. Chem. 41 (1998) 640–649.
[9] A.D. Abell, G.J. Foulds, J. Chem. Soc., Perkin Trans. 1 (1997) 2475–2482.
[10] W.G. Finnegan, R.A. Henry, R. Lofquist, J. Am. Chem. Soc. 80 (1958) 3908–3911.
[11] M.E. Wolff, Burger's Medicinal Chemistry, Part III, John Wiley & Sons, California, 1996. pp. 300–305.
[12] R.C. Elderfield, Tetrazoles, Tetrazines and Purines and Related Ring Systems, Heterocyclic Compounds, vol. 8, John Wiley & Sons Inc., New York, 1981. pp. 2–105.
[13] T.L. Gilchrist, Pyrazoles, Triazoles, and Tetrazoles Heterocyclic Chemistry, Cambridge University Press, Cambridge, 1976. pp. 195–204.
[14] P. Pulay, G. Fogarasi, G. Pongor, J.E. Boggs, A. Vargha, J. Am. Chem. Soc. 105 (1983) 7037–7047.
[15] M.J. Frisch, G.W. Trucks, H.B. Schlegel, G.E. Scuseria, M.A. Robb, J.R. Cheeseman, G. Scalmani, V. Barone, B. Mennucci, G.A. Petersson, H. Nakatsuji, M. Caricato, X. Li, H.P. Hratchian, A.F. Izmaylov, J. Bloino, G. Zheng, J.L. Sonnenberg, M. Hada, M. Ehara, K. Toyota, R. Fukuda, J. Hasegawa, M. Ishida, T. Nakajima, Y. Honda, O. Kitao, H. Nakai, T. Vreven, J.A. Montgomery, Jr., J.E. Peralta, F. Ogliaro, M. Bearpark, J.J. Heyd, E. Brothers, K.N. Kudin, V.N. Staroverov, R. Kobayashi, J. Normand, K. Raghavachari, A. Rendell, J.C. Burant, S.S. Iyengar, J. Tomasi, M. Cossi, N. Rega, J.M. Millam, M. Klene, J.E. Knox, J.B. Cross, V. Bakken, C. Adamo, J. Jaramillo, R. Gomperts, R.E. Stratmann, O. Yazyev, A.J. Austin, R. Cammi, C. Pomelli, J.W. Ochterski, R.L. Martin, K. Morokuma, V.G. Zakrzewski, G.A. Voth, P. Salvador, J.J. Dannenberg, S. Dapprich, A.D. Daniels, O. Farkas, J.B. Foresman, J.V. Ortiz, J. Cioslowski, D.J. Fox, Gaussian 09, Revision B.01, Gaussian Inc., Wallingford, CT, 2010.
[16] P. Hohenberg, W. Kohn, Phys. Rev. 136 (1964) B 864–B 871.
[17] W. Kohn, L. Sham, Phys. Rev. 140 (1965) A1133–A1138.
[18] Spartan 10, Wavefunction Inc., Irvine, CA 92612, USA, 2010.
[19] G. Rauhut, P. Pulay, J. Phys. Chem. 99 (1995) 3093–3100.
[20] M.T. Güllüoğlu, Y. Erdogdu, J. Karpagam, N. Sundaraganesan, Ş. Yurdakul, J. Mol. Struct. 990 (2011) 14–20.
[21] Y. Erdogdu, M.T. Güllüoğlu, Ş. Yurdakul, Ö. Dereli, Opt. Spectrosc. 113 (2012) 23–32.
[22] Y. Erdogdu, D. Manimaran, M.T. Güllüoğlu, M. Amalanathan, I. Hubert Joe, Ş. Yurdakul, Opt. Spectrosc. 114 (2013) 46–57.
[23] Y. Erdogdu, Spectrochim. Acta A 106 (2013) 25–33.
[24] H. Ozisik, S. Saglam, S.H. Bayari, Struct. Chem. 19 (2008) 41–50.
[25] S. Bayarı, S. Saglam, H.F. Ustundag, J. Mol. Struct. THEOCHEM 726 (2005) 225–232.
[26] S.H. Bayari, B. Seymen, H. Ozisik, S. Saglam, J. Mol. Struct. THEOCHEM 893 (2009) 17–25.
[27] T.R. Sertbakan, S. Saglam, E. Kasap, Z. Kantarci, J. Mol. Struct. 482 (1999) 75–79.
[28] C.N.R. Rao, R. Venkataraghavan, Can. J. Chem. 42 (1964) 43–49.
[29] J. Svetlik, A. Martvon, J. Lesko, Chem. Zvesti. 33 (1979) 521–527.
[30] S. Subashchandrabose, R. Akhil, H. Krishnan, V. Saleem, V. Thanikachalam, G. Manikandan, Y. Erdogdu, J. Mol. Struct. 981 (2010) 59–70.
[31] Y. Erdogdu, M.T. Güllüoğlu, M. Kurt, J. Raman Spectrosc. 40 (2009) 1615–1623.